Kinetic Control of Interparticle Spacing in Au Colloid-Based Surfaces: Rational Nanometer-Scale Architecture

Katherine C. Grabar, Patrick C. Smith, Michael D. Musick, Jennifer A. Davis, Daniel G. Walter, Michael A. Jackson, Andrea P. Guthrie, and Michael J. Natan*

Contribution from the Department of Chemistry, The Pennsylvania State University, 152 Davey Laboratory, University Park, Pennsylvania 16802

Received July 7, 1995[⊗]

Abstract: This paper details the kinetic aspects of covalent self-assembly of colloidal Au particles from solution onto immobilized organosilane polymers. On glass substrates, surface formation can be monitored using UV−vis spectroscopy and field emission scanning electron microscopy (FE-SEM). Correlation of these data allows the effect of nanostructure on bulk optical properties to be evaluated. At short derivatization times, particle coverage is proportional to (time)$^{1/2}$. The particle sticking probability p, defined as the ratio of bound particles to the number of particles reaching the surface in a given time period, can be determined from a knowledge of the particle radius, solution concentration, temperature, and solution viscosity; for surfaces derivatized with (3-mercaptopropyl)-trimethoxysilane (MPTMS), $p \approx 1$. At longer derivatization times, interparticle repulsions result in a "saturation" coverage at ≈30% of a close-packed monolayer. Two approaches for modulating the rate of surface formation are described: electrochemical potential control on organosilane-modified SnO_2 electrodes and charge screening by organic adsorbates. Self-assembly of colloidal Au particles onto functionalized substrate surfaces is a reproducible phenomenon, as evidenced by UV−vis and surface enhanced Raman scattering (SERS) measurements on identically prepared substrates.

Introduction

Elaboration of the novel physical, optical, and chemical attributes of particles with submicron dimensions represents a crowning achievement in materials chemistry.[1−6] To harness these interesting properties within macroscopic devices requires large numbers of particles. As such, assembly of individual nanometer-scale particles into ensembles has recently become an important and widely-pursued objective. In many cases, the desired architecture consists of two-dimensional arrays of particles supported on a substrate.[7−21] However, little information exists on the factors that govern nanostructure within this geometry. In particular, the rates of particle-array formation, the significance of interparticle forces, and the approaches to controlling those forces have not been addressed.

Reported herein is a detailed study on the kinetics of colloidal Au particles binding to organosilane-coated transparent substrates. We have previously described how macroscopic, self-assembling Au and Ag surfaces can be prepared by covalent attachment of colloidal Au to functional groups on surface-confined organosilanes (Scheme 1).[22,23] This flexible approach to Au particle films yields substrates which are active for surface enhanced Raman scattering (SERS), support electrochemical measurements, can be selectively coated with Ag, and can be made in large numbers.[22−25] Recently, work along similar lines by the groups of Cotton and Willner has appeared.[26,27]

The focus here is on the factors that govern the particle distribution on the surface. Using UV−vis spectroscopy and FE-SEM, we show that at early times (t), surface assembly is under kinetic control, with the particle coverage well-described by a simple $t^{1/2}$ dependence. At later times, Au colloid coverage is limited by repulsive interparticle interactions that effectively

* Author to whom correspondence should be addressed: E-Mail natan@chem.psu.edu.

[⊗] Abstract published in *Advance ACS Abstracts,* January 15, 1996.

(1) Steigerwald, M. L.; Brus, L. E. *Acc. Chem. Res.* **1990**, *23*, 183−188.
(2) Wang, Y.; Herron, N. *J. Phys. Chem.* **1991**, *95*, 525−532.
(3) (a) Henglein, A. *J. Phys. Chem.* **1993**, *97*, 5457−5471. (b) Henglein, A. *Chem. Rev.* **1989**, *89*, 1861−1873.
(4) Weaver, J. H.; Waddill, G. D. *Science* **1991**, *251*, 1444−1451.
(5) Hageld, A.; Gratzel, M. *Chem. Rev.* **1995**, *95*, 49−68.
(6) (a) Martin, C. R. *Science* **1994**, *266*, 1961−1966. (b) Martin, C. R. *Acc. Chem. Res.* **1995**, *28*, 61−68.
(7) Facci, P.; Erokhin, V.; Tronin, A.; Nicolini, C. *J. Phys. Chem.* **1994**, *98*, 13323−13327.
(8) Lazarov, G. S.; Denkov, N.; Velev, O. D.; Kralchevsky, P. A.; Nagayama, K. *J. Chem. Soc., Faraday Trans.* **1994**, *90*, 2077−2083.
(9) Wang, J.-Q.; Xiao, G. *Phys. Rev. B* **1995**, *51*, 5863−5867.
(10) Morneau, A.; Manivannan, A.; Cabrera, C. R. *Langmuir* **1994**, *10*, 3940−3942.
(11) Asher, S. A.; Holtz, J.; Liu, L.; Wu, Z. *J. Am. Chem. Soc.* **1994**, *116*, 4997−4998.
(12) Leon, R.; Petroff, P. M.; Leonard, D.; Fafard, S. *Science* **1995**, *267*, 1966−1968.
(13) Colvin, V. L.; Goldstein, A. N.; Alivisatos, A. P. *J. Am. Chem. Soc.* **1992**, *114*, 5221−5230.
(14) Röder, H.; Hahn, E.; Brune, H.; Bucher, J.-P.; Kern, K. *Nature* **1993**, *366*, 141−143.
(15) Weaver, J. H.; Waddill, G. D. *Science* **1991**, *251*, 1444−1451.
(16) Douglas, K.; Devaud, G.; Clark, N. A. *Science* **1992**, *257*, 642−644.
(17) Yang, J.; Fendler, J. H. *J. Phys. Chem.* **1995**, *99*, 5505−5511.
(18) Ford, W. E.; Rodgers, M. A. J. *J. Phys. Chem.* **1995**, *99*, 5139−5145.
(19) Flood, R. U.; Fitzmaurice, D. *J. Phys. Chem.* **1995**, *99*, 8954−8958.
(20) Boonekamp, E. P.; Kelly, J. J.; Fokkink, L. G. J. *Langmuir* **1994**, *10*, 4089−4094.
(21) Lassaletta, G.; Fernández, A.; Espinós, J. P.; González-Elipe, A. R. *J. Phys. Chem.* **1995**, *99*, 1484−1490.
(22) Freeman, R. G.; Grabar, K. C.; Allison, K. J.; Bright, R. M.; Davis, J. A.; Guthrie, A. P.; Hommer, M. B.; Jackson, M. A.; Smith, P. C.; Walter, D. G.; Natan, M. J. *Science* **1995**, *267*, 1629−1632.
(23) Grabar, K. C.; Freeman, R. G.; Hommer, M. B.; Natan, M. J. *Anal. Chem.* **1995**, *67*, 735−743.
(24) Bright, R. M.; Walter, D. G.; Musick, M. D.; Jackson, M. A.; Allison, K. J.; Natan, M. J. *Langmuir* In press.
(25) Grabar, K. C.; Allison, K. A.; Baker, B. E.; Bright, R. M.; Brown, K. R.; Dolan, C. M.; Freeman, R. G.; Fox, A. P.; Musick, M. D.; Natan, M. J. *Langmuir* Accepted for publication.
(26) Chumanov, G.; Sokolov, K.; Gregory, B. W.; Cotton, T. M. *J. Phys. Chem.* **1995**, *99*, 9466−9471.
(27) Doron, A.; Katz, E.; Willner, I. *Langmuir* **1995**, *11*, 1313−1317.

0002-7863/96/1518-1148$12.00/0

Scheme 1

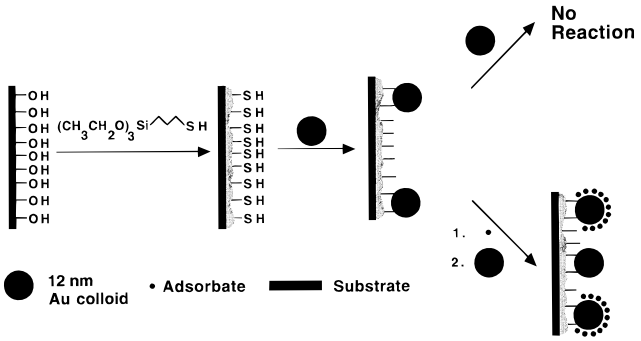

inhibit additional particle immobilization. Importantly, this repulsive interaction can be partially screened by organic adsorbates. This technique is used to prepare surfaces that are highly reproducible for surface enhanced Raman scattering (SERS).

The utility of nanoparticle-based devices, and particularly those based on self-assembly, will ultimately hinge on repeatable device performance, and this in turn depends on fully reproducible nanostructures. For colloidal Au, an understanding of the kinetic factors involved in surface construction has allowed such structures to be realized.

Experimental Section

Materials. The following materials were obtained from Aldrich: $HAuCl_4 \cdot 3H_2O$, trisodium citrate dihydrate, poly(vinylpyrrolidone) (PVP), and *trans*-1,2-bis(4-pyridyl)ethylene (BPE). $HOCH_2CH_2SH$ was purchased from Sigma. 2-(Trimethoxysilyl)ethyl-2-pyridine (PETMS) was obtained from Hüls America, Inc. The following compounds were obtained from United Chemical Technologies: (3-aminopropyl)-trimethoxysilane (APTMS), (3-aminopropylmethyl)diethoxysilane (APMDES), (3-mercaptopropyl)trimethoxysilane (MPTMS), and ((3-mercaptopropyl)methyl)dimethoxysilane (MPMDMS). Concentrated H_2SO_4 was purchased from J. T. Baker Inc., and 30% H_2O_2 was obtained from VWR. CH_3OH (spectrophotometric grade) was obtained from EM Science; all H_2O was 18 MΩ, distilled through a Barnstead Nanopure H_2O purification system. BPE was recrystallized several times from a mixture of H_2O and CH_3OH; other materials were used as received. Glass microscope slides were obtained from Fisher Scientific, and Sb-doped SnO_2 (100 $\Omega \cdot cm^2$) from Delta Technologies.

Colloid Preparation. Colloidal Au particles were prepared by citrate reduction of $HAuCl_4$ in aqueous solution.[23,28] Average particle diameters were consistently in the range of 12−15 nm with standard deviations of 2−4 nm. Particle sizes were determined by analysis of transmission electron microscopy (TEM) photographs using the public-domain software NIH Image.[29]

Substrate Derivatization. All substrates were cleaned in a "piranha" bath[30] (30% H_2O_2 mixed in a 1:4 ratio with concentrated H_2SO_4 at 60 °C) prior to derivatization. Glass substrates were immersed in CH_3OH or hexane solutions containing 1−10% organosilane for time periods of 5 min to 24 h. Details of these procedures can be found in the supporting information. SnO_2 surfaces were fabricated into electrodes and silanized in a 1% (w/w) solution of organosilane in H_2O as described previously.[24]

For the APTMS-derivatized surfaces that were treated with colloidal Au and with either 4 mM trisodium citrate, 4 mM BPE, 4 mM PVP, or 4 mM $HSCH_2CH_2OH$, the following procedure was used. (i) Substrates were immersed in colloidal Au for a given time period and rinsed with H_2O. (ii) Substrates were immersed in adsorbate solutions for 8 min and again rinsed with H_2O, after which an optical spectrum was recorded in H_2O. (iii) The sample was reimmersed in colloidal Au and the cycle repeated. For SERS reproducibility measurements, MPMDMS-derivatized surfaces were coated sequentially in colloidal Au (16 h), 1 mM BPE (10 min), colloidal Au (1 h), 1 mM BPE (10 min), and colloidal Au (30 min); substrates were rinsed with H_2O between each step. A Pine RDE4 bipotentiostat was used for electrochemical experiments.

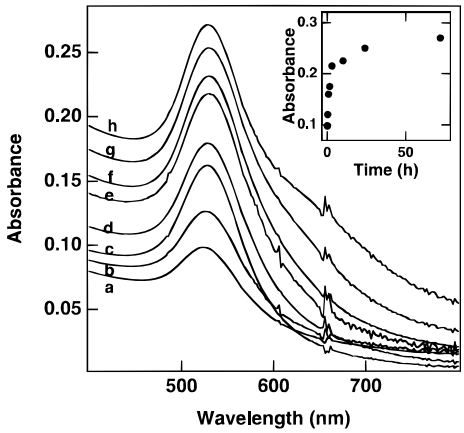

Figure 1. Optical spectra for MPTMS-coated glass slides derivatized in colloidal Au for (a) 5 min, (b) 15 min, (c) 45 min, (d) 90 min, (e) 3 h, (f) 10 h, (g) 1 day, and (h) 3 days. Inset: Increase in absorbance at λ_{max} as a function of time.

Image and Data Analysis. FE-SEM micrographs were digitally converted to their negative images and adjusted for optimum contrast prior to analysis and presentation. For the determination of particle coverage and placement, it was occasionally necessary to separate particles that were touching by drawing a line of width 1−2 nm between adjacent particles. Analysis areas were typically 1020 nm × 720 nm. Particles in the outer 40-nm shell of this box were only considered in determining nearest-neighbor distances of particles in the inner box. The same methods were used for computer-generated random distributions of particles on a 15.4 μm × 15.4 μm surface; in this case, the excluded shell was 200 nm. Non-linear least-squares fits were carried out using a commercial software implementation of the Levenberg-Marquardt algorithm.

Instrumentation. FE-SEM data was obtained using a JEOL JSM-6320F instrument, equipped with an in-lens detector and operated at 3 kV accelerating voltage. Other instrumentation has been described previously.[22−25] Single diode-based data spikes at ≈656 nm in UV−vis data were artificially removed.

Results and Discussion

Kinetics of Surface Formation. The high-extinction surface plasmon resonance of colloidal Au[31] allows particle immobilization on transparent substrates to be followed directly by UV−vis spectroscopy. Figure 1 shows the evolution of Au colloid-based films on a set of MPTMS-coated glass slides immersed in a solution of 15-nm-diameter Au particles for varying lengths of time. The optical spectrum (in H_2O) of an MPTMS/glass slide after a 5-min immersion leads to an easily observed absorbance peak at 524 nm.[32] This feature grows in rapidly for slides exposed to Au for 1−2 h. Surprisingly, the absorbance of slides derivatized for longer times essentially saturates. The abrupt nature of this transition is illustrated in the inset to Figure 1, which plots peak absorbance at λ_{max} vs time. During the time period from 3 to 72 h, the increase in absorbance is only half that observed during the first 3 h of Au colloid

(28) Frens, G. *Nature Phys. Sci.* **1973**, *241*, 20−22.

(29) Written by Wayne Rasband at the U.S. National Institutes of Health and available from the Internet by anonymous FTP from zippy.nimh.nig.gov or on floppy disk from NTIS, 5285 Port Royal Rd., Springfield, VA, 22161, part number PB93-504868.

(30) **Caution!** Piranha solutions are extraordinarily dangerous, reacting explosively with trace quantities of organics. They should be handled in very small quantities with the utmost care.

(31) Bohren, C. T.; Huffman, D. R. *Absorption and Scattering of Light by Small Particles*; Wiley: New York, 1983.

(32) For small Au particles, visible light extinction is dominated by absorbance.[33] Therefore, the latter term is used exclusively here.

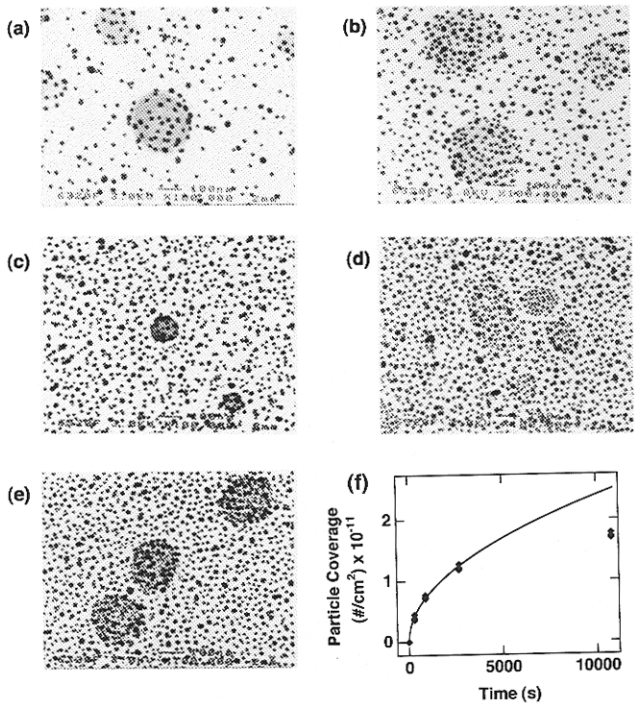

Figure 2. (a−e) FE-SEM images (1.15 μm × 0.9 μm) of MPTMS-coated glass slides derivatized in 15-nm-diameter colloidal Au for (a) 5 min (0.39×10^{11} particles/cm^2), (b) 15 min (0.73×10^{11} particles/cm^2), (c) 45 min (1.22×10^{11} particles/cm^2), (d) 3 h (1.6×10^{11} particles/cm^2), and (e) 3 d (1.82×10^{11} particles/cm^2). (f) Particle coverage vs immersion time for 15-nm-diameter colloidal Au. The solid line is the best fit to [particle coverage/cm^2] = $(2.39 \times 10^9)t^{1/2}$, where the coeffecient comes from a nonlinear least-squares fit to all data points before 4000 s.

immobilization. Derivatization for longer periods of time—up to 6 weeks—results in no substantial increase in absorbance.

Determination of the nanometer-scale structure of the samples described in Figure 1 is essential for two reasons. First, it provides an experimental framework for correlating nanostructure with bulk optical properties. There are several approaches to well-defined Au or Ag nanostructures,[33−39] but none in which the feature size can be fixed and the feature spacing varied in real time. Second, for surfaces with uniform nanostructure, it paves the way for the use of UV−vis as a nanostructure probe. Figure 2 shows five ≈1-μm^2 FE-SEM images obtained from samples used to generate the data in Figure 1. These images are representative of areas four times those shown.

Careful inspection reveals a number of important features about Au colloid-based surface formation. The lowest-coverage data (a) indicate that particles are randomly bound to the surface. This contrasts sharply with electrophoretically-deposited colloidal Au films described by Giersig and Mulvaney,[40] in which an attractive force between Au particles even at low coverages is manifested through the presence of close-packed, ordered structures. Here, strong covalent bonds between organosilane sulfhydryl groups and the colloid surface prevent particle migration on the organosilane film. Consistent with the optical spectra in Figure 1, increased immersion times lead to increased numbers of isolated partices, rather than three-dimensional clusters, which are easily discerned by FE-SEM.[25]

The spherical regions of darker background observed in some of these images are attributable to unevenly polymerized organosilane. This assignment is confirmed by their presence in samples not coated with colloidal Au (supporting information). Depending on the conditions used for organosilane film formation, these semi-translucent features cover from 0 to 20% of the surface and are roughly 250 nm in diameter (supporting information). These organosilane particles also serve as templates for Au colloid immobilization, yielding coverages 2−2.5 times greater than adjacent, planar regions. Considering the increased surface area of a partly truncated sphere relative to the corresponding plane, Au colloid coverages on the spherical particles are similar to the organosilane thin films.

Plots of overall particle coverge versus immersion time (Figure 2f) mirror the steep rise and subsequent plateau depicted in Figure 1 for sample absorbance. Quantitative characterization of these data is available through use of equations that describe diffusion of spherical particles to a planar surface. Following the treatment of Park et al.,[41−42] eq 1 relates q, the number of

$$q = 0.163pnyt^{1/2} \quad (1)$$

particles reaching a 1-cm^2 surface per unit time, to p (a sticking probability), n (particle concentration in number/cm^3), y (a constant incorporating particle radius, viscosity, and temperature), and t (time in seconds). Coverage values over the first 45 min are nicely fit using non-linear least squares to the equation $2.39 \times 10^9\ t^{1/2}$ (solid line in Figure 2f), but data at later times fall significantly below this curve.

Both the early-time agreement and long-time deviations from predicted coverages are significant. The $t^{1/2}$ adherence of particle immobilization at early times means that even without knowledge of particle size or concentration in solution, relative particle coverages can be calculated based on derivatization times: a 4-fold increase in coating time results in twice the number of immobilized particles. If n and y are known, independent measurement of q at a time t yields p, the sticking probability. In other words, p is the ratio of number of particles bound to the number that reached the surface, and its value conveys kinetic information about substrate−colloid interactions. Using the fit data in Figure 2f, and assuming completely monodisperse 15-nm-diameter particles, a sticking probability of 1.2 ± 0.4 is calculated.[43] This rather large error reflects the extreme sensitivity of this calculation to particle size as well as the error associated with the best-fit data. Given these uncertainties, it is difficult to report an exact value for p, but it is safe to say that the sticking probability of colloidal Au to organosilane polymers with pendant sulfhydryl groups is very high.

Deviation from $t^{1/2}$ dependence at higher particle coverages must result from changes in n or p since the other variables in eq 1 are constant over time. Because only 1% of the total colloid concentration is surface bound for the coverages shown

(33) Blatchford, C. G.; Campbell, J. R.; Creighton, J. A. *Surf. Sci.* **1982**, *120*, 435−455.
(34) Van Duyne, R. P.; Hulteen, J. C.; Treichel, D. A. *J. Chem. Phys.* **1993**, *99*, 2101−2115.
(35) Semin, D. J.; Rowlen, K. L. *Anal. Chem.* **1994**, *66*, 4324−4331.
(36) Liao, P. F.; Bergman, J. G.; Chemla, D. S.; Wokaun, A.; Melngailis, J.; Hawyrluk, A. M.; Economou, N. P. *Chem. Phys. Lett.* **1981**, *82*, 355−359.
(37) Liao, P. F.; Stern, M. B. *Opt. Lett.* **1982**, *7*, 483−485.
(38) Meier, M.; Wokaun, A.; Vo-Dinh, T. *J. Phys. Chem.* **1985**, *89*, 1843−1846.
(39) Foss, C. A. J.; Hornyak, G. L.; Stockert, J. A.; Martin, C. R. *J. Phys. Chem.* **1994**, *98*, 2963−2971.
(40) Giersig, M.; Mulvaney, P. *J. Phys. Chem.* **1993**, *97*, 6334−6336.
(41) Park, K.; Simmons, S. R.; Albrecht, R. M. *Scanning Microsc.* **1987**, *1*, 339−350.
(42) Park, K.; Park, H.; Albrecht, R. M. In *Colloidal Gold: Principles, Methods and Applications*; Hayat, M. A., Ed.; Academic Press: San Diego, 1989; Vol. 1, Chapter 18.
(43) With $T = 293$ K, particle diameter = 15 nm, particle concentration = 8.86 nM, and viscosity = 0.01002 g/(cm·s), $q_{calc} = (1.98 \times 10^9)pt^{1/2}$. Therefore, $p = 2.38 \times 10^9/1.98 \times 10^9 = 1.2$.

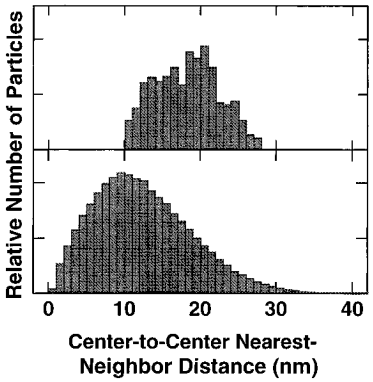

Figure 3. Top: Center-to-center nearest-neighbor distances for Au particles (1.6×10^{11}/cm^2) bound to an MPTMS-coated glass slide. Distances reflect an analysis area of 1.04 μm x 740 nm taken from Figure 2d. Bottom: Center-to-center distances for random particle distributions at a coverage of 1.6×10^{11}/cm^2, in which particle overlap is allowed.

in Figure 2f, a change in n can immediately be ruled out. Thus, the sticking probability must be lower at higher coverages. This is a reasonable conclusion given the decrease in the number of available binding sites on the surface as particle coverage increases.[44]

Comparison of experimental particle spacings on these surfaces with a randomly generated particle distribution supports the premise that interparticle repulsion determines final surface coverage. Center-to-center nearest-neighbor spacings were tabulated for a substrate immersed in colloid for 3 h, the first datum that falls significantly below the $t^{1/2}$ curve in Figure 2f. The coverage on this sample was 1.6×10^{11} particles/cm^2. Figure 3 compares the experimentally-derived spacings (top) with those of a random distribution of 15-nm particles at the same coverage, in which particle overlap was allowed, i.e. particles are allowed to stack on top of each other without any interparticle repulsion (bottom). This phenomenon is quite prevalent in the simulated data, in which >50% of the particles are in partial or full contact with another (i.e. nearest-neighbor distance <15 nm). In contrast, the real data show a much narrower distribution, centered about a spacing twice as great as for the simulated data. Moreover, when one considers that a distribution in particle sizes artificially broadens nearest-neighbor histograms (center-to-center spacings <15 nm are possible only with particles whose diameters are <15 nm; similarly, larger particles lead to larger apparent spacings), the difference between the real and simulated data is even more dramatic. Essentially, the same repulsive forces that keep colloidal Au apart in solution prohibit a close packing of particles on the surface. At coverages greater than $\geq 1.2 \times 10^{11}$ particles/cm^2, this leads to absorbance plateaus (Figure 1), negative deviations from $t^{1/2}$ kinetics, and higher mean interparticle spacings.

(44) One quantitative approach to understanding the coverage dependence of p is based upon a classical kinetic model for surface adsorption.[45] According to this model, $p = r \exp[-E/kT]$, where r accounts for the fact that all particle−surface collisions may not result in binding (i.e. a particle in solution may collide with another surface-bound particle rather than a region of organosilane), k is Boltzmann's constant, T is temperature in degrees K, and E is the energy barrier to binding. While colloidal Au represents only 30% of the total surface area, the percentage of non-contact sites available for 15-nm particles is far less than 70%. Thus r decreases with increasing coverage (at $t = 0$, $r = 1$; at longer times, $r \approx 0$). While at low coverages ($p \approx 1$ ($\approx r$)) E must necessarily be quite small, it is likely that at higher coverages, the activation energy for particle binding increases due to interparticle repulsion. Surface coating does proceed more rapidly at 70 °C than at 20 °C (supporting information), but decreased viscosity and increased temperature account for most of this change.

(45) Gardiner, W. C., Jr. *Rates and Mechanisms of Chemical Reactions*; W. A. Benjamin, Inc.: Menlo Park, 1972; pp 181−183.

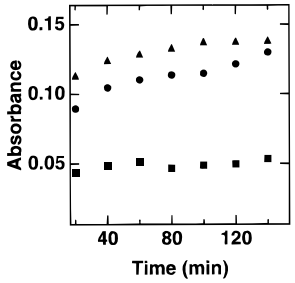

Figure 4. Absorbance vs time for an APMDES-coated SnO_2 electrode in the presence of 17 nM, 12-nm-diameter colloidal Au and held at open circuit (▲), at +0.3 V vs SCE (●), and at −0.3 V vs SCE (■).

Modulation of Surface Formation Rate. Equally important as the finding that Au colloid monolayer coverages are limited at early times by diffusion and at later times by interparticle repulsion are experiments that demonstrate that these effects can be modulated. Colloidal Au derived from $[AuCl_4]^-$ has an intrinsic fixed negative charge resulting from strongly adsorbed Cl^- and/or a coating of $[AuCl_2]^-$ (produced by incomplete reduction of $[AuCl_4]^-$).[46] Action of an electric field on this charge should modulate particle flux to a surface. Accordingly, three APMDES-coated SnO_2 electrodes were immersed in a solution of 17 nM, 12-nm-diameter colloidal Au. Using a bipotentiostat, electrochemical potentials of two electrodes were held simultaneously at +0.3 V and −0.3 V vs SCE, with the third not under potential control. Representative plots of absorbance (at open circuit) vs time for the three electrodes are shown in Figure 4. The electrode held at −0.3 V vs SCE exhibits substantially less colloidal Au derivatization per unit time, while that held at +0.3 V vs SCE coats at a slightly lower rate than the open-circuit electrode. This experiment has been repeated several times, with slight differences in relative rates. In each case, however, the open circuit electrode coated fastest, and the electrode at −0.3 V vs SCE coated most slowly. The rate of surface formation at open circuit also exceeded the rate for electrodes held at +0.5, +0.1, −0.1, and −0.5 V vs SCE.

These data can be explained through electric-field-induced changes in particle migration and immobilization kinetics. At open circuit, mass transfer toward the electrode surface occurs by diffusion and, at close range, by electrostatic attraction to the fixed positive charges associated with surface-confined protonated amines. Introduction of an electric field via an electrochemical potential places a charge on the electrode and generates a double layer of charge at the interface. When the electrode is held at negative potentials, this charge is negative and therefore repulsive, leading to a reduced particle flux relative to open circuit. The lower coating rate at negative potentials is thus expected. At positive potentials, the charge is positive and attractive, leading to an increased flux relative to open circuit. Nevertheless, fewer colloidal Au particles actually bind to the surface per unit time, suggesting that the presence of a double layer kinetically inhibits colloidal Au immobilization, possibly via screening of amine−Au interactions.

Screening of the repulsive force between colloidal Au particles is possible with strong adsorbates. The concept behind such an experiment is shown in the right side of Scheme 1. The basic idea is that Au colloid submonolayers that have reached repulsion-limited coverage can be induced to bind more particles if the repulsive influence of surface-bound particles is first screened by interaction with strong adsorbates. The results of such an experiment are shown in Figures 5 and 6 for four

(46) Handley, D. A. In *Colloidal Gold: Principles, Methods and Applications*; Hayat, M. A., Ed.; Academic Press: San Diego, 1989; Vol. 1, Chapter 1.

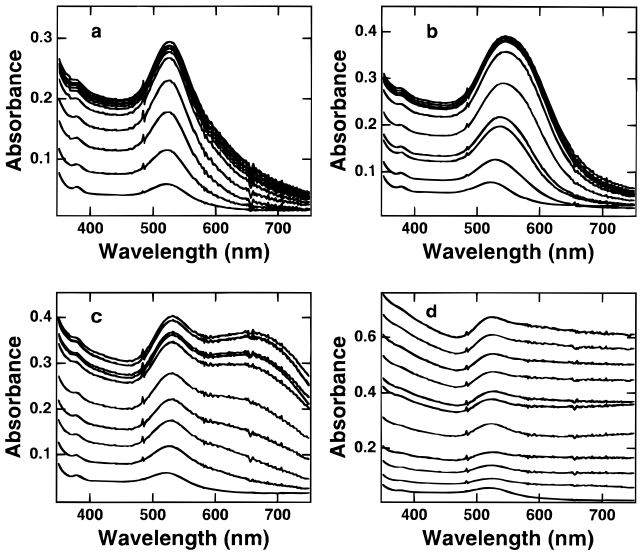

Figure 5. Absorbance spectra for APTMS-coated glass slides coated alternately in colloidal Au and (a) 4 mM sodium citrate, (b) 4 mM PVP, (c) 4 mM BPE, or (d) 4 mM $HOCH_2CH_2SH$. Optical spectra were recorded after each iteration of Au/adsorbate coatings, and reflect total immersion times in colloidal Au of 5, 10, 20, 30, 60, 90, 120, 150, 180, 210, and 240 min. Each substrate immersion in solutions containing adsorbate was for 8 min.

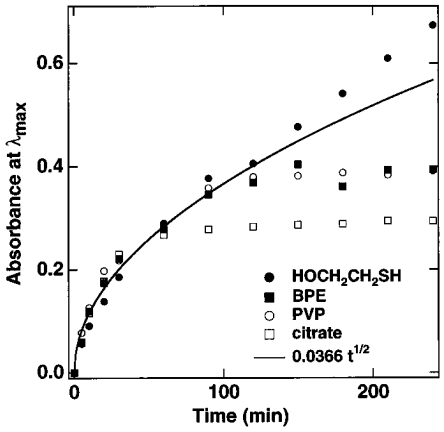

Figure 6. Absorbance at λ_{max} versus immersion time for each of the adsorbate-treated systems shown in Figure 5. The solid line is the nonlinear least-squares best fit to the first 7 data points for $HOCH_2CH_2SH$, BPE, and PVP and the first 5 data points for citrate.

different adsorbates: PVP, BPE, citrate, and $HOCH_2CH_2SH$. APTMS-coated glass slides were immersed in solutions of 12-nm-diameter colloidal Au for 5 min. After rinsing, they were placed in 4 mM solutions of the adsorbates for 8 min and then rinsed. Optical spectra were measured in H_2O, and this cycle was repeated with increasing immersion times in colloidal Au, until the total time in colloidal Au solution was 240 min. The optical spectra for the slide treated with citrate is shown in Figure 5a, with PVP in Figure 5b, BPE in Figure 5c, and $HOCH_2CH_2SH$ in Figure 5d. Plots of absorbance values at λ_{max} as a function of time are plotted for each data set in Figure 6.

Analysis of these data validates the idea that molecular adsorption effectively screens interparticle repulsion between surface-confined Au nanoparticles. Moreover, the data show that Beer's law holds for colloidal Au submonolayers. These conclusions obtain as follows: (1) Absorbance data acquired over the first hour from all four adsorbates is well fit by a *single* $t^{1/2}$ curve. The data of Park et al.[42−43] and that shown in Figure 2f relate coverage to time; this kinetic analysis has not been previously applied to a macroscopic parameter such as absorbance. As expected, diluted solutions of colloidal Au are also fit by a similar equation over longer times. In each case, the same overall coverage is attained. (2) The fact that absorbance data follow $t^{1/2}$ proves that *in this regime*, a linear relationship exists between particle coverage and absorbance (i.e. Beer's law holds).[47] It can therefore be stated that *coverages* on all four slides follow the expected behavior over the first hour. Clearly, molecular adsorption has no consequence over this period. (3) Repeated immersion in 4 mM citrate has no effect on coverage at longer times; repulsion-limited coverage is reached in the first hour, and coverage does not increase afterward. In contrast, both PVP and BPE-treated samples continue to bind colloidal Au after the first hour. Importantly, coverage increases with a $t^{1/2}$ dependence, showing that interparticle repulsion is still not operative. Thus, these two adsorbates effectively screen forces that are otherwise present (i.e. with citrate or without any adsorbate). However, for both PVP and BPE, a new, higher repulsion-limited plateau in coverage is reached after roughly 2 h. (4) When repulsive interactions are completely screened, the ability to prepare single layers of particles is compromised: for $HOCH_2CH_2SH$, the high background and low-energy extinction visible in the optical spectra in Figure 5 are consistent with formation of aggregates.[22−25] Evidently, barriers to both covalent surface attachment and particle−particle agglomeration have been overcome. As a result, the positive deviation from predicted coverages at long times reflects absorbance contributions from species other than isolated individual particles.

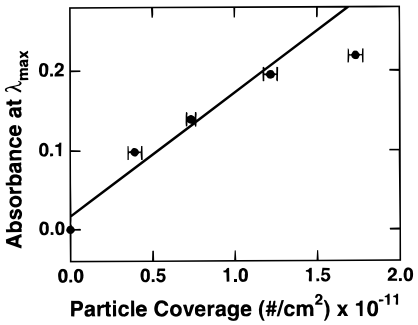

Figure 7. Absorbance versus particle coverage for 15-nm-diameter Au colloids on MPTMS-derivatized glass. Errors in absorbance are smaller than the dot size.

Absorbance vs coverage data indicate that close proximity of *isolated* particles also impacts light extinction by colloidal particles, leading to deviation from Beer's law behavior. Figure 7 shows a plot of absorbance versus particle coverage taken from the data in Figures 1 and 2. The first few data points give a reasonably good fit to a straight line (correlation coefficient = 0.98). Using the analysis of Bohn and co-workers,[48] a per-particle surface extinction coefficient (ϵ_{surf}) of 9.3×10^8 M^{-1} cm^{-1} is calculated.[49] However, the first coverage that deviates from $t^{1/2}$ behavior (10 800 s; 1.7×10^{11} particles/cm^2) also deviates from Beer's law, and this trend is continued at higher coverages. It is unclear whether these phenomena

(47) Given a coverage $\Gamma = k_1 t^{1/2}$, where k_1 is a constant, if A vs t data are fit by a $t^{1/2}$ curve, then $A = k_2 t^{1/2}$, where k_2 is a constant. Substituting in for $t^{1/2}$ yields the expression $A = (k_2/k_1)\Gamma$. Thus, A is a linear function of Γ.

(48) Hong, H.; Bohn, P. W.; Sligar, S. G. *Anal. Chem.* **1993**, *65*, 1635−1638.

(49) Using a least-squares algorithm, a best-fit line to data points up to 1.2×10^{11} particles/cm^2 yielded a slope and intercept of 0.1556×10^{-11} and 0.0168, respectively. From Bohn's work,[48] surface absorbance is defined in relation to the surface extinction coefficient and the particle coverage (number/cm^2) as follows: $A_{surf} = \Gamma\epsilon_{surf}/(6.02 \times 10^{20})$. Thus, the following relationship exists between the best-fit line slope and the surface extinction coefficient: $0.1556 \times 10^{-11} = \epsilon_{surf}/(6.02 \times 10^{20})$; thus, $\epsilon_{surf} = 9.3 \times 10^8$ M^{-1} cm^{-1}.

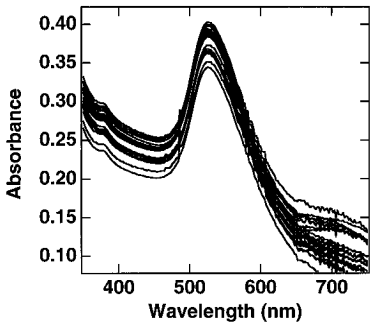

Figure 8. Absorbance spectra for 24 simultaneously-prepared samples of colloidal Au (28 ± 4 nm diameter)/PETMS/glass.

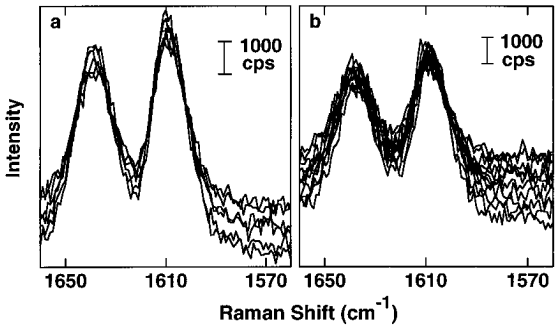

Figure 9. (a) SERS spectra of BPE ring-stretching modes at (a) 6 different locations on a single 12-nm-diameter Au/MPMDMS/glass substrate and (b) 10 different simultaneously-prepared samples. Acquisition parameters: 20-mW 632.8-nm excitation, 1-cm^{-1} step, 1-s integration, 5-cm^{-1} band-pass.

are related, but it is tempting to speculate that ϵ_{surf} is sensitive to the presence of local charge on adjacent particles.

Without absolute particle coverages, an exact sticking probability for 12-nm colloidal Au to amine-terminated organosilanes cannot be calculated. It can, however, be estimated using the fit data from Figure 6, ϵ_{surf} for 15-nm-diameter Au particles, and the fact that particle extinction scales with cross-sectional area. A surface extinction coefficient for 12-nm Au particles of 5.9×10^8 M^{-1} cm^{-1} is calculated, leading to a p of 1.1. Once again, the approximate nature of these calculations limits the accuracy of these measurements; all that can be stated with confidence is that amine groups bind colloid Au with a roughly equal (high) avidity as do sulfhydryl groups. This contrasts with data from cyanide-bearing organosilanes, for which the sticking probabilities are much lower. To achieve similar coverages as mercapto- or aminosilanes would therefore require much longer immersion times. One key difference between RCN, RSH, and RNH_2 is that the former functional group is not ionized in the pH 4−10 regime. This leads to a hydrophobic interface and creates a barrier to binding of charged particles suspended in aqueous solution.

It should be noted that the present inability to calculate precise values for *p* in no way lessens the chemical significance of these measurements. The sticking probability is an important probe of particle−surface interactions, and experiments designed to yield more accurate values are underway.

Reproducibility. Reproducibility of bulk properties is a critical yardstick for monitoring control over interparticle spacing in Au colloid assemblies. Figure 8 shows the optical spectra for 24 simultaneously prepared Au colloid monolayers on PETMS-coated glass slides. The lack of a significant peak in the 600−700-nm region suggests that on every surface, the colloidal particles are relatively far apart. More importantly, there are only small changes (7%) in the overall absorbance (and therefore, coverage), and these are not corrected for errors associated with sampling area and sample tilt in the cuvette.

SERS spectra, collected from a line focus of 1 mm × 3 mm, were acquired at several spots on a given Au colloid-based surface. These data, along with that obtained on several different surfaces, are shown in Figure 9. In all cases, spectra were acquired from samples in cuvettes of 1 mM BPE. For each of the 6 spots, there are only small differences in SERS intensity; similarly, high reproducibility was obtained for SERS spectra measured on 10 identically prepared substrates. These data were not corrected for errors associated with sample positioning and fluctuations in laser power; thus, the true substrate reproducibility is higher than its appearance here.

Conclusions

This paper has for the first time considered kinetic aspects of surface formation by nanoparticle self assembly from solution. For covalent attachment of colloidal Au to surface-confined organosilane films, the following key points were demonstrated. (i) At early times, colloidal Au binds to random sites on MPTMS- or APTMS-coated substrates. (ii) A very high percentage of particle−surface collisions lead to particle immobilization. (iii) Particle coverage and absorbance both exhibit a $t^{1/2}$ dependence, and Beer's law is followed for surface-confined particles. (iv) As derivatization time increases beyond the first hour, both the absorbance and the particle coverage deviate from $t^{1/2}$ behavior and reach a plateau level, i.e. "saturation". Analyses of interparticle spacings at these coverages indicate that repulsive forces govern particle assembly beyond the early-time, diffusion-dominated regime. (v) Further evidence for this interaction comes from experiments in which particle coverage was varied by adsorption of charge-screening adsorbates. (vi) Control of particle size and interparticle spacing leads to surfaces with reproducible SERS and UV−vis spectra.

This study provides a framework for production of colloidal Au surfaces with extremely well-defined nanometer-scale architectures. Accordingly, these surfaces are now being evaluated for a number of applications (e.g. direct electrochemistry of metalloproteins).[50] It is important to point out that the methods described herein for predicting, measuring, and tuning the rate of colloidal Au immobilization are applicable to other nanoparticles; such information will be invaluable as the demand for designed, self-assembling nanostructured materials increases.

Acknowledgment is made to the National Science Foundation (CHE 92-08614, CHE 92-56692, and CHE-9307485) and the Beckman Foundation for partial support of this research, as well as to the Eastman Kodak Company for a graduate fellowship to K.C.G. Acknowledgment is also made to the Electron Microscopy Facility for the Life Sciences in the Biotechnology Institute at The Pennsylvania State University. We thank the Jurs group at Penn State for help with computer simulations, JEOL USA, Inc. for FE-SEM analyses, and a reviewer for helpful comments regarding Figure 3.

Supporting Information Available: FE-SEM images of MPTMS- and APTMS-coated glass substrates with and without colloidal Au; absorbance vs time plot showing the effect of temperature on coating rate; experimental details on substrate derivatization methods (3 pages). This material is contained in many libraries on microfiche, immediately follows this article in the microfilm version of the journal, can be ordered from the ACS, and can be downloaded from the Internet; see any current masthead page for ordering information and Internet access instructions.

JA952233+

(50) Brown, K. R.; Fox, A. P.; Natan, M. J. *J. Am. Chem. Soc.* **1996**, *118*, 1154−1157.